A new misfit function for multimodal inversion of surface waves

Margherita Maraschini[1], Fabian Ernst[2], Sebastiano Foti[3], and Laura Valentina Socco[1]

ABSTRACT

Higher-mode contribution is important in surface-wave inversion because it allows more information to be exploited, increases investigation depth, and improves model resolution. A new misfit function for multimodal inversion of surface waves, based on the Haskell-Thomson matrix method, allows higher modes to be taken into account without the need to associate experimental data points to a specific mode, thus avoiding mode-misidentification errors in the retrieved velocity profiles. Computing cost is reduced by avoiding the need for calculating synthetic apparent or modal dispersion curves. Based on several synthetic and real examples with inversion results from the classical and the proposed methods, we find that correct velocity models can be retrieved through the multimodal inversion when higher modes are superimposed in the apparent dispersion-curve or when it is not trivial to determine a priori to which mode each data point of the experimental dispersion curve belongs. The main drawback of the method is related to the presence of several local minima in the misfit function. This feature makes the choice of a consistent initial model very important.

INTRODUCTION

Dispersion of Rayleigh and Scholte waves can be used to estimate an S-wave velocity model, which is helpful for several near-surface applications, for designing filters to remove ground roll from seismic reflection records, and for calculating the statics in seismic reflection processing (Mari, 1984).

Dispersion-curves can be estimated using several spectral analysis techniques (Dziewonski and Hales, 1972; Nolet and Panza, 1976; McMechan and Yedlin, 1981) aimed at retrieving the fundamental and higher modes of surface-wave propagation in a wide frequency band. Park et al. (1998) and Luo et al. (2008) propose, respectively, a wavefield transformation and a high-resolution linear Radon transform to improve modal Rayleigh-wave separation.

In surface-wave inversion, we should take into account higher modes because, in several real cases, the experimental dispersion curve is the result of the superposition of several modes, particularly when velocity inversions or strong velocity contrasts are present in the S-wave profile. Higher modes are sensitive to parameters to which the fundamental mode is poorly sensitive (Socco and Strobbia, 2004); so, considering them in the inversion process can improve the accuracy of the result (Ernst, 2008; Maraschini et al., 2008), especially in the presence of a velocity decrease with depth (Gucunski and Woods, 1992; Xia et al., 2003). Including higher modes can increase the investigation depth (Gabriels et al., 1987) when the low-frequency band is not available (Ernst, 2008), can stabilize the inversion process (Xu et al., 2006), and can enhance the resolution of the inverted model.

Several authors propose inversion schemes that allow multimodal inversion. Gabriels et al. (1987) propose a least-squares multimodal inversion that minimizes the distance between calculated modal curves and experimental dispersion-curve branches. Rayleigh-wave inversion using higher modes is presented by Tokimatsu et al. (1992) and Tokimatsu (1997), highlighting that errors can be made in the inversion if the observed dispersion curve is compared only to the theoretical fundamental mode, particularly in the case of irregular velocity profiles. The inversion process used by Park et al. (1999) consists of a preliminary inversion using the fundamental mode, with a successive refinement of the results made by comparing the higher modes with the observed dispersion curves. Xu et al. (2006) describe from a theoretical perspective a multichannel method that is more flexible than traditional methods, discriminating and integrating fundamental and higher modes of Rayleigh waves. Song and Gu (2007) invert multimodal dispersion curves, relative to sites with low-velocity layers, by means of a genetic algorithm using a multimodal inversion that minimizes a weighted sum of the least-squares error for each mode.

All of this work demonstrates the importance of higher modes in

Rayleigh-wave inversion, but it also highlights that including them in the inversion presents difficulties. One problem to deal with is the separation and identification of different modes in the spectrum. This can be done only if many sensors and a long array are available (Foti 2000; Foti et al., 2002); whereas when a two-station acquisition geometry is considered, only an apparent dispersion curve can be identified (Tokimatsu et al., 1992; Tokimatsu, 1997). Gabriels et al. (1987) present an example of using a long array to identify different modes.

Even if higher-mode branches are retrieved experimentally, the main difficulty is that all of these approaches require identifying the mode number for each data point. Zhang and Chang (2003) show that mode-misidentification errors on the experimental dispersion-curve, particularly at low frequencies, often are greater than errors resulting from inaccurate data for a given mode. On the other hand, Zhang and Chang (2003) highlight that the difficulty in including higher modes in the inversion is due to the absence of a generic relationship between the fundamental and the higher modes. Moreover, it is difficult to determine the mode order of the data points in several situations; when it is not possible to enumerate the modes correctly, standard multimodal approaches can lead to incorrect results.

Some authors solve this problem performing the inversion by calculating an apparent dispersion curve, i.e., the observed Rayleigh-wave velocity is the result of the superposition of several modal curves. Calculating the apparent dispersion curve implies the need for a realistic simulation of the propagated wavefield that accounts for the source parameters, the sampling, and all factors that cause attenuation.

An automated procedure to invert the apparent dispersion-curve is reported by Ganji et al. (1998). Forbriger (2003a, 2003b) also describes a procedure that accounts for higher modes. He shows that the procedure is robust and produces better results than conventional techniques when several modes are present in the data set. This procedure avoids the inversion using modal curves because it uses the full waveform, including higher and leaky modes with their amplitudes. Lai and Rix (1999) propose inverting multimodal dispersion-curves without assigning a mode number to data points, based on the calculation of an apparent dispersion-curve obtained by superimposing modal displacements. Also, Lu and Zhang (2006) apply a genetic algorithm that compares, for each frequency, the observed dispersion curves and the modal curve associated with the maximum displacement. This inversion is slower but more stable than least-squares multimodal inversion because it avoids modal misidentification. Ryden and Park (2006) invert the phase-velocity spectrum of data to avoid the necessity of numbering different modes. These methods, which invert the spectrum or the apparent dispersion-curve, require the displacement calculation; consequently, they are more complicated and computationally expensive than methods based on modal dispersion curves.

We propose a deterministic multimodal inversion of Rayleigh and Scholte waves that is able to account for modal superposition without the need to calculate the apparent dispersion curve. It also allows several branches of the dispersion curve to be inverted simultaneously without the need of associating them to a specific mode number. Our approach considers a new misfit based on the implicit function whose zeros are modal curves. The approach of minimizing the determinant of the stiffness matrix has been suggested by Ernst (2007); we apply the same idea to the Haskell-Thomson method. Such a misfit does not require the dispersion-curve calculation; consequently, it reduces the computational cost for the misfit evaluation.

After presenting the approach, we apply it to synthetic and field data, comparing our results with classical dispersion-curve inversion. We show different examples of synthetic and real data in which the experimental curve is the result of modal superposition or where different dispersion-curve branches, related to higher modes, are retrieved.

METHOD

Misfit function

We consider two different misfit functions to solve the inverse problem (Maraschini, 2008; Maraschini et al., 2008).

We first introduce the forward problem. The vectorial space $\mathbf{m}$ contains all possible models; its dimension is the number of model parameters $N_{\mathbf{m}}$; $\mathbf{m}$ is the generic element of $\mathbf{M}$. We consider a subsoil model given by a stack of linear elastic homogeneous layers. Model parameters are S-wave velocity, P-wave velocity (or Poisson's ratio), thickness, and density of each layer.

The space $\mathbf{D}$ is the vectorial space of data whose dimension is $N_{\mathbf{d}}$; $\mathbf{d}$ is the generic element of $\mathbf{D}$. Data $\mathbf{d} = (V,f)$ is a point in the velocity-frequency (V-f) domain:

$$\mathbf{D}^{\text{obs}} = \begin{bmatrix} V_1^{\text{obs}} & f_1^{\text{obs}} \\ \vdots & \vdots \\ V_N^{\text{obs}} & f_N^{\text{obs}} \end{bmatrix}.$$

The matrix contains all observed data points $\mathbf{d}^{\text{obs}}$, i.e., the ith line of the matrix contains the frequency and the velocity of the ith data point; N is the number of data points.

The forward operator used in this paper is the Haskell-Thomson transfer matrix method (Thomson, 1950; Haskell, 1953, 1964), as modified by Gilbert and Backus (1966) and subsequently by Dunkin (1965), Herrmann and Wang (1980), and Herrmann (2002). Our approach can be applied more generally to the whole class of propagator matrix methods, such as the reflection-transmission matrix method (Kennett, 1974; Kennett and Kerry, 1979) and the stiffness matrix method (Kausel and Roesset, 1981). Moreover, the same method can be used for inversion of all surface and interface waves (e.g., Love waves).

The matricial Haskell-Thomson method builds a homogeneous system. The system matrix $\mathbf{T}$ is the product of several matrices, one for each subsoil layer and others for boundary-condition implementation (Buchen and Ben-Hador, 1996). This system has a nontrivial solution if and only if the determinant of $\mathbf{T}$ is zero. The determinant of $\mathbf{T}$ depends on the model $\mathbf{m}$ and on the point (V,f); consequently,

$$\left| \mathbf{T}(V,f,\mathbf{m}) \right| = 0 \tag{1}$$

represents the forward operator.

For a given model $\mathbf{m}*$, the curves such that $\left| \mathbf{T}(V,f,\mathbf{m}*) \right| = 0$ are the possible solutions of the problem, i.e., a certain frequency component of the surface waves with frequency $f*$ can travel only with velocity values V_i such that $\left| \mathbf{T}(V_i,f*,\mathbf{m}*) \right| = 0$. These curves are called modes of the dispersion curve.

Figure 1 shows an example of the function $\left| \mathbf{T}(V,f,\mathbf{m}*) \right|$ and the related modal curves for a given model $\mathbf{m}*$. The surface is continuous and smooth. The zeros of this surface are the modal curves of the model, and the value of the surface increases when the distance from the modal curves increases. This function does not present other zeros than the modal curves.

The classical misfit function minimizes the geometric distance between the real and synthetic dispersion-curves:

$$S(\mathbf{m}) = \left\{ \sum_{i=1}^{N} [w_i |V_i^{obs} - g(\mathbf{m}|f_i^{obs})|]^\ell \right\}^{1/\ell}, \qquad (2)$$

where w_i represents the weight of the ith point; $g(\mathbf{m}|f_i^{obs})$ represents the forward operator, which calculates the velocity value of a given mode (chosen by the user) of the dispersion curve at the ith frequency; and ℓ is the considered norm. This approach requires mode numbering.

In Figure 2, the observed dispersion curve is represented by black dots, and the experimental dispersion curve is represented by the green line. The misfit is the norm of the vector containing the distance between the observed and the synthetic dispersion curves points for the frequency of the observed data (vertical dotted line).

The shape of the function $|\mathbf{T}(V,f,\mathbf{m}*)|$ (Figure 1) suggests to use it as an alternative misfit function to the classical one. The real data points should respect the condition $|\mathbf{T}(V_i,f,\mathbf{m}*)| = 0$; thus, our approach searches a synthetic model such that the value of the $\mathbf{T}$ surface is as low as possible at the data points. The proposed misfit function, referred to as the determinant misfit function, is the norm of the vector containing the value of the $\mathbf{T}$ surface evaluated at the experimental data points:

$$S(\mathbf{m}) = \left\{ \sum_{i=1}^{N} [w_i |\mathbf{T}(V_i^{obs},f_i^{obs},\mathbf{m})|]^\ell \right\}^{1/\ell}, \qquad (3)$$

where w_i represents the weight of the ith point, the function $\mathbf{T}$ is the determinant of the Haskell-Thomson forward modeling evaluated at each ith point, and ℓ is the considered norm.

This misfit function allows all modes to be considered because all modal curves are minima of the surface. When several branches of dispersion curves are retrieved, they all can be inverted simultaneously without the need for associating them with a specific mode.

An important aspect of the determinant misfit function is related to apparent dispersion-curve inversion. The $\mathbf{T}$ surface assumes low values in the region of the velocity-frequency (V-f) domain where the apparent dispersion curve can pass from one mode to another. An example is shown in Figure 1, where the $\mathbf{T}$ function presents low values at low frequency, allowing a smooth transition from fundamental to first higher mode. This feature is important when the retrieved experimental curve is an apparent curve generated by modal superposition; it can pass from one mode to a higher one, crossing a region that does not belong to any modal curve. The value of the $\mathbf{T}$ function is very low in this region, so the misfit associated to the considered model is low and the inversion can converge easily to a final model that produces modal superposition. We can therefore invert apparent dispersion curves without the need to simulate the apparent dispersion curve itself.

In Figure 3, we show the calculation of the determinant misfit distance; black dots represent an experimental dispersion curve, and the colored area is the surface that represents the absolute value of the Haskell-Thomson matrix determinant of a given model $\mathbf{m}*$ evaluat-

ed for each V-f pair [calculated with the forward operator $\mathbf{T}(V,f,\mathbf{m}*)$]. If the model $\mathbf{m}*$ was correct, the black dots would have corresponded to the zeros of the surface. The determinant misfit distance minimizes the values assumed by the surface in correspondence to the real points. In Figure 3c, the experimental points lie on the plane where the determinant modulus is zero; the vertical distance between each experimental point and the surface represents the misfit on the point. The norm of the vector containing the misfit values on experimental points is the misfit of $\mathbf{m}*$. No normalization process is applied to the misfit value.

The determinant approach does not require the zero search because the dispersion curves are not explicitly calculated; consequently, the computing cost of the misfit evaluation is reduced with respect to the classical approach. Moreover, all modes are considered without the need to specify to which mode each point belongs.

The algorithm allows uncertainties to be taken into account. Data uncertainties define the data weights w_i, i.e., a point with high uncertainty is associated with a low weight, and vice versa. In the following examples, uncertainties are not taken into account.
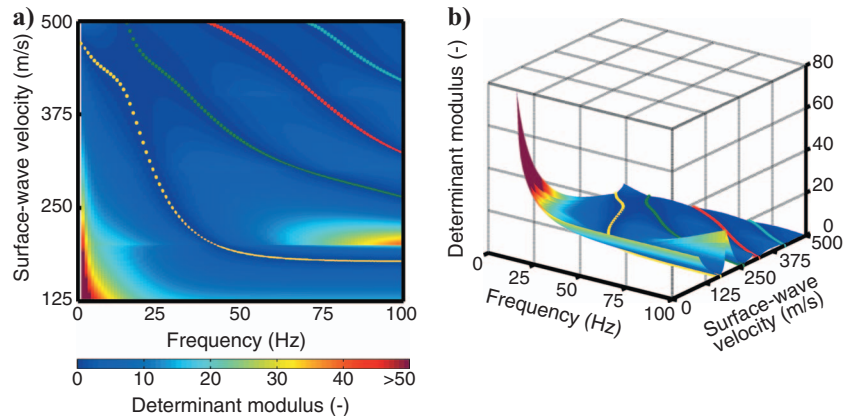

Figure 1. Absolute value of the Haskell-Thomson determinant for a given model (three layers over a half-space, water layer on the top of the model). Colored dots represent the modal curves that correspond to the zeros of the determinant. The minima of the surface correspond to the dispersion curves of the model: (a) 2D view; (b) 3D view.
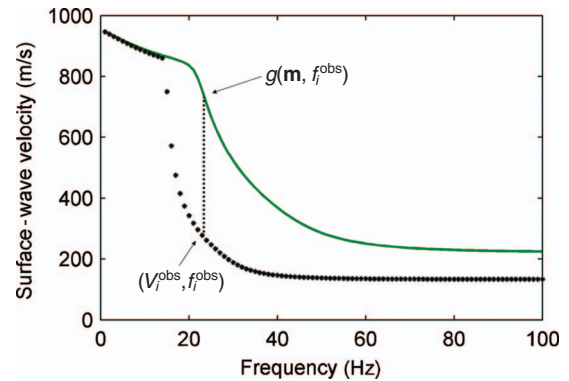

Figure 2. Calculation of the classical misfit function. The green line represents the synthetic dispersion curve, and the black dots represent the experimental data. For each frequency, the corresponding distance is the difference between the velocities of the two curves.

Inversion algorithm

We have implemented a deterministic inversion based on the steepest-descent method (Tarantola, 2005) with the quasi-Newton metric matrix. The inversion algorithm is the same for the two approaches, except for calculating the misfit function.

In the classical approach, the misfit function is the norm of the distances between the real and the synthetic dispersion curves. If more than one branch is present in the experimental dispersion curve, each branch is compared to a specific mode of the synthetic dispersion curve.

In the determinant approach, the misfit function is the norm of the absolute value of the determinant of the Haskell-Thomson matrix of the synthetic model evaluated on real data points. When more than
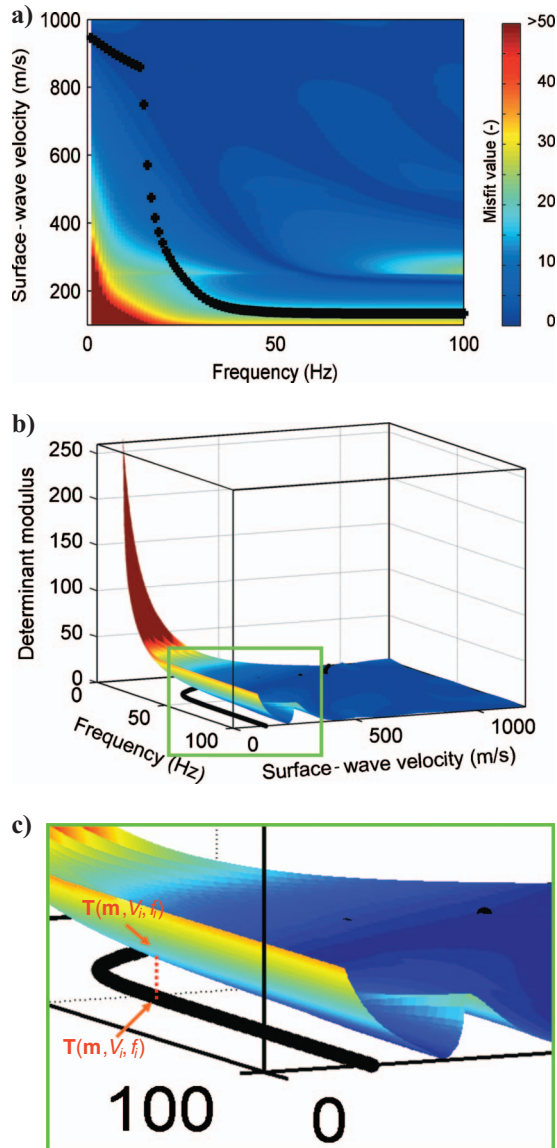

Figure 3. Calculation of the determinant misfit function. The colored surface represents the absolute value of the Haskell-Thomson matrix determinant of the synthetic model. The black dots represent the experimental data. For each experimental point, the corresponding distance is the value assumed by the surface at the same V-f pair: (a) 2D view, (b) 3D view, (c) close-up of 3D view.

one branch is present in the observed data, the procedure is the same because all modes are minima of the modulus of the Haskell-Thomson matrix determinant, without the need for associating each branch to a specific mode of the synthetic dispersion curve.

The inversions are performed on the thicknesses and on the S-wave velocity of each layer and the S-wave velocity of the half-space, assuming a priori the values for density and Poisson's ratio (or P-wave velocity). The algorithm starts from an initial model $\mathbf{m}_0$, and the model is updated at each iteration following the gradient of the misfit function:

$$m_{k+1}^\alpha = m_k^\alpha - \mu_k f^{\alpha\beta}(\mathbf{m}_k)\left(\frac{\partial S}{\partial m^\beta}\right)_k, \qquad (4)$$

where m_k^α is component α of the model vector at iteration k, μ_k is a real factor chosen to help convergence, $f_{\alpha\beta}(\mathbf{m}_k)$ is the metric matrix in the space of parameters, and $f^{\alpha\beta}$ is the metric matrix in the dual space of the parameter space, i.e., $f_{\alpha\sigma}f^{\sigma\beta} = \delta_\alpha^\beta$, where δ_α^β represents the identity matrix. The Newton method uses the Hessian matrix of the misfit function as the metric matrix on the space of parameters (it is possible because it is positive definite):

$$f_{\alpha\beta}(\mathbf{m}) = \left(\frac{\partial^2 S}{\partial m^\alpha \partial m^\beta}(\mathbf{m})\right)_\mathbf{m}. \qquad (5)$$

The algorithm is implemented for a generic norm, but our results are obtained using the L^1-norm.

If several branches of the dispersion curve are available, the inversion is performed using two steps. At first, only the slowest branch is considered. After a few iterations, higher branches are also included.

In deterministic inversion, the initial model should be close to the solution to avoid local minima. This feature is particularly important in the case of a deterministic algorithm based on the determinant misfit function; all of the modes are minima of the misfit function, so it is important to start from a velocity profile close to the true one to avoid fitting the apparent dispersion curve with an incorrect mode. In particular, if the initial model velocities are strongly underestimated, the algorithm may converge to an incorrect solution, overestimating the mode numbering.

SYNTHETIC AND EXPERIMENTAL EXAMPLES

In this section, we compare determinant inversion with classical inversion using synthetic and experimental data. To make the results comparable, in all examples we inverted the data using the same deterministic algorithm and the same initial model; only the misfit functions differ. The determinant and the classical inversion algorithms have been implemented on purpose for this paper.

We generated the two synthetic data sets using a finite-difference code (case 1) and a finite-element code (produced by Comsol; case 2) to simulate seismic records for a layered linear elastic system. The source is a Ricker wavelet (10-Hz dominant frequency), and the seismic data are the time histories of the vertical displacement at the free surface. The model characteristics are summarized in Table 1, and the simulation parameters are summarized in Table 2. Land and

marine real data are acquired for different purposes and with different equipment and geometry; acquisition parameters are noted in Table 3.

We retrieved the dispersion curves for synthetic and real data using a MATLAB code that calculates the *f-k* spectrum of the seismic data, searches the maxima of the amplitude spectrum, and transforms the *f-k* coordinates of the maxima to the phase velocity-frequency domain. The maxima search was performed in spectral regions selected by the operator after visual data evaluation. This allowed several branches of the dispersion curve to be retrieved. For the classical inversion, the different branches need to be associated with a specific mode; therefore, they were numbered (the slowest branch associated to the fundamental mode, the second branch to the first higher mode, etc.). Note that the determinant inversion requires careful processing and data evaluation, as does the classical approach.

The choice of the initial model is a critical task for deterministic inversion — particularly for the determinant approach — because the misfit presents several local minima. For the synthetic and real data, the initial model was chosen considering the slowest branch of the apparent dispersion-curve in a new domain, velocity-wavelength/2.5- (or V-$\lambda/2.5$), discretizing it with a minimum parameterization criterion (Foti, 2000). The velocity values obtained for the

shallower layers were then increased slightly to avoid local minima in the determinant inversion. When more than one branch of the apparent dispersion-curve was available, both inversions were performed first considering only the slowest branch and then all available branches.

Synthetic data

Two-mode synthetic data (case 1)

We obtained these data by simulating the propagation on a simple model made of a soft layer overlying a stiff bedrock (Table 1). We show the synthetic seismogram and the frequency-wavenumber (*f-k*) spectrum in Figure 4. The retrieved dispersion curve presents three branches and has a frequency band of $5-25$ Hz. The slowest branch of the retrieved dispersion curve is the result of modal superposition and presents a smooth passage from the fundamental mode to the first higher mode at low frequency. In real data, this can be easily encountered, and often only the slowest branch of dispersion curve is retrieved. Therefore, we analyze these data in two steps. In the first step, we consider only the slowest branch of the dispersion curve, and we invert it using both the classical and the determinant approaches; then we repeat the inversion using all branches. In the classical inversion, the slowest branch of the apparent dispersion curve is considered the fundamental mode (because it is impossible to identify a jump on a higher mode from the apparent dispersion curve), whereas no assumption on the mode numbering is made for the determinant inversion.

In Figure 5a, we show the slowest branch of the synthetic dispersion curve (velocity versus $\lambda/2.5$), the initial model, the true model, and the results of classical and determinant inversions. In Figure 5b, we show the apparent dispersion curve retrieved from the *f-k* spectrum and the theoretical modal curves calculated from the two final models. The result obtained through the classical inversion is affected by a strong overestimation of the half-space velocity. This is be-

Table 1. Characteristics of the synthetic models.

Model	Layer	Density (kg/m³)	Poisson's ratio (−)	S-wave velocity (m/s)	Thickness (m)
1	1	1800	0.33	150	10
1	2	2100	0.27	450	90
2	1	1800	0.33	150	10
2	2	2000	0.27	280	20
2	3	2100	0.27	450	770

Table 2. Modeling parameters.

Model	Model length (m)	Receiver spacing (m)	Source depth (m)	Time window (s)	Time sampling (s)	Number of elements	Element shape	Geometry
1	1500	5	0	6	0.001	600,000	Quadrangular	2D axial-symmetric
2	2000	5	30	4	0.001	22,208	Triangular	2D axial-symmetric

Table 3. Field data acquisition parameters.

Data set	Array length (m)	Receiver type	Receiver spacing (m)	Source type	Acquisition time (s)	Time sampling (ms)	Number of receivers
Case A	6000	Hydrophone	12.5	Airgun	6.0	4.0	480
Case B	48	Vertical 4.5 Hz	2	Drop weight	0.512	0.25	24
Case C	16.4	Vertical 4.5 Hz	0.7	Hammer	0.512	0.25	24

cause the apparent dispersion curve is the result of modal superposition and includes the contribution of a higher mode at low frequency.
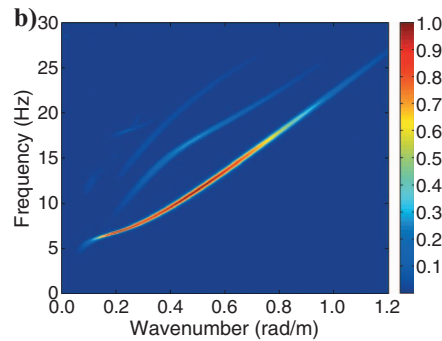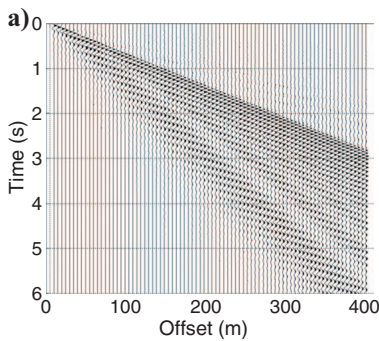

Figure 4. Representation of the seismogram and corresponding *f-k* spectrum for synthetic case 1: (a) synthetic seismogram; (b) *f-k* spectrum of the seismogram.
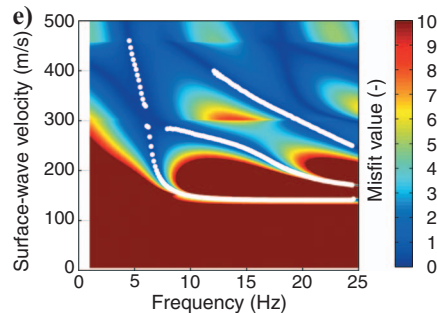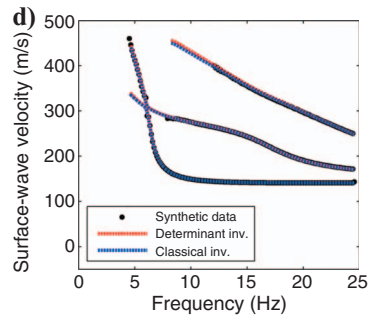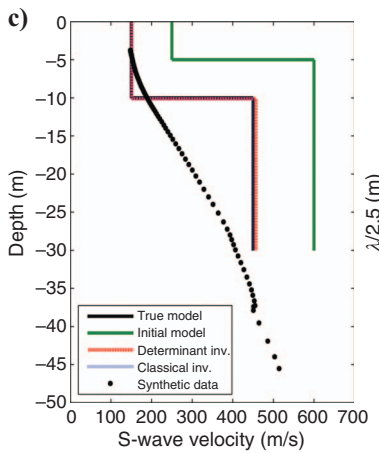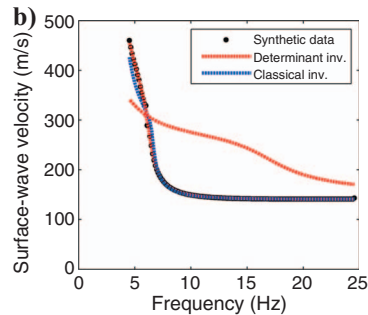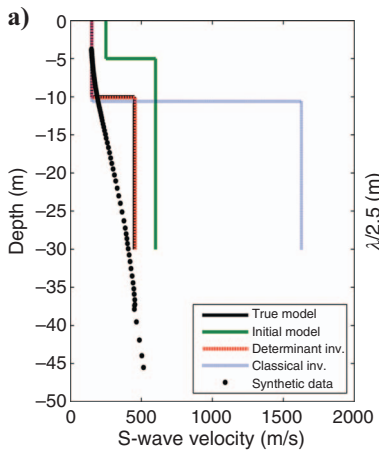

Figure 5. Inversion results for synthetic case 1. (a) The S-wave velocity profiles for the inversion of the slowest branch of the dispersion curve compared with the first branch of the synthetic data ($\lambda/2.5$-V domain). (b) Dispersion curves for inverting the slowest branch of the dispersion curve. (c) S-wave velocity profiles for the inversion of all curve branches compared with the first branch of the synthetic data (classical inversion is coincident with the true model). (d) Dispersion curves for the inversion of all curve branches. (e) Synthetic dispersion-curve compared with the misfit function of the determinant inversion.

Inverting the data through the determinant approach, we obtain a final result that agrees with the true model. The apparent dispersion-curve fits the first higher mode in the low-frequency band and the fundamental mode in the higher-frequency band. The determinant inversion algorithm converges toward the correct solution because the solution that involves the fundamental and the first-higher mode presents a minimum of the misfit function (Figure 5e). Note that we did not introduce a priori information to force the inversion toward a higher mode.

When we inverted the data with the classical inversion, comparing the retrieved dispersion curve with the fundamental mode, we made a wrong assumption about the data. In real cases, this is a common pitfall; because the pattern of the retrieved dispersion curve is smooth and continuous, there is no way to recognize that part of the dispersion curve is in fact related to higher modes of propagation. Moreover, even after the inversion, it is not easy to realize that a mistake was made because the data fitting can be good with a fundamental-mode curve relative to a wrong model.

We then inverted the data also considering the other branches of dispersion curve. For the classical inversion, the slowest branch of the apparent dispersion curve is considered the fundamental mode, the second branch is considered the first higher mode, and the third branch is considered the second higher mode; no assumption on mode numbering is made for the determinant inversion.

In Figure 5c, we show the slowest branch of the synthetic dispersion-curve (velocity versus $\lambda/2.5$), the initial model, the true model, and the results of the classical and determinant inversions. In Figure 5d, we show the apparent dispersion-curves and the modal curves obtained by the final models of the two inversions. Figure 5e compares the Haskell-Thomson surface of the final model of the determinant inversion to the apparent dispersion curve. In this case, the two inversions retrieve similar results: the result obtained by the determinant inversion is not improved by the higher modes because it was already close to the true profile, but the result obtained by the classical inversion is strongly improved by including higher modes.

We performed a parametric analysis on this data set to show the importance of the choice of the initial model. Figure 6a shows the result of the parametrical analysis performed on the classical misfit using only the slowest branch of the apparent dispersion-curve associated with the fundamental mode. The normalized misfit presents only one region with a low misfit value. It corresponds to the correct value of the S-wave velocity of the first layer (150 m/s), mainly related to the high-frequency band of the dispersion-curve, but it is unable to properly constrain the value of the

S-wave velocity of the half-space related to the low-frequency band. The misfit value indeed decreases when the half-space S-wave velocity increases, bringing the classical inversion to converge to an incorrect result. When higher modes are also considered in the classical inversion, the minimum of the misfit function corresponds to the true values of the S-wave velocities (Figure 6b).

We show the sensitivity analysis of the determinant approach in Figure 6c. The normalized misfit presents several local minima, corresponding to different values of the S-wave velocity of the shallow layer. The correct solution corresponds to the global minimum of the normalized misfit, and this feature makes the algorithm converge to the correct solution. The presence of several local minima emphasizes the need for a careful choice of the initial model.

In the determinant multimodal inversion, the relation between model parameters and misfit value is more complicated than in the classical inversion. Observing Figures 6a and b, we can clearly see that the misfit presents only one minimum, which, in Figure 6b, corresponds to the correct solution. On the other hand, several local minima are present in the determinant misfit (Figure 6c). This feature is related strictly to the mode numbering, which is not required. For the classical inversion, each experimental point should correspond to a given mode; for the determinant inversion, the experimental points could correspond to any mode.

In this example, the determinant misfit presents local minima corresponding to several values of the S-wave velocity of the first layer. These minima correspond to fitting the high-frequency part of the dispersion-curve with the fundamental mode (higher S-wave velocity value), the first higher mode, the second, and so on. One way to avoid local minima is therefore to start the inversion from a model whose first-layer velocity is higher than the true velocity because there are no local minima with first-layer velocity higher than the true one (Figure 6c). The true velocity is unknown, so we assume as a reference the velocity of the experimental dispersion curve at high frequency (short wavelength).

These considerations hold for a synthetic model composed of one layer over a half-space and fixing the layer thickness to the correct value; when more complicated models are considered, sensitivity analysis becomes multidimensional. In general, when the experimental dispersion curve presents phase velocity increasing with wavelength, the proposed practical rule for the initial model (higher velocity at high frequency) produces good results. For the synthetic example, we ran the inversion starting from several initial models with the first-layer velocity higher than the reference velocity. The results are shown in Figure 7. All considered initial models allow the algorithm to converge to models close to the correct solution.

Multimode synthetic data (case 2)

We obtained these data for a synthetic model made of two layers over a half-space (Tables 1 and 2), applying the seismic source on the top of the half-space. By positioning the source at depth, we obtained a synthetic data set where several higher modes can be retrieved in addition to the fundamental mode.

Figure 8 shows the synthetic seismogram and the f-k spectrum. Several dispersive events related to the propagation of higher modes are clearly evident in the f-k spectrum. Searching for the relative amplitude maxima, we could retrieve the fundamental mode plus eight branches of higher modes. We show the retrieved dispersion curve in Figure 9b. Note that the frequency band within which we could retrieve the fundamental mode is limited to $2-8$ Hz, whereas the high-

er-mode dispersion-curve branches span the frequency band up to 32 Hz. Therefore, accounting for higher modes implies an improvement in the amount of available information.

Both classical and determinant approaches are illustrated in Figure 9. Data fitting of the classical inversion is good; for the first four modes, the correspondence between the number of the branch of the apparent dispersion curve and the number of the mode is correct. At the fourth branch, there is a mode jump; consequently, from that
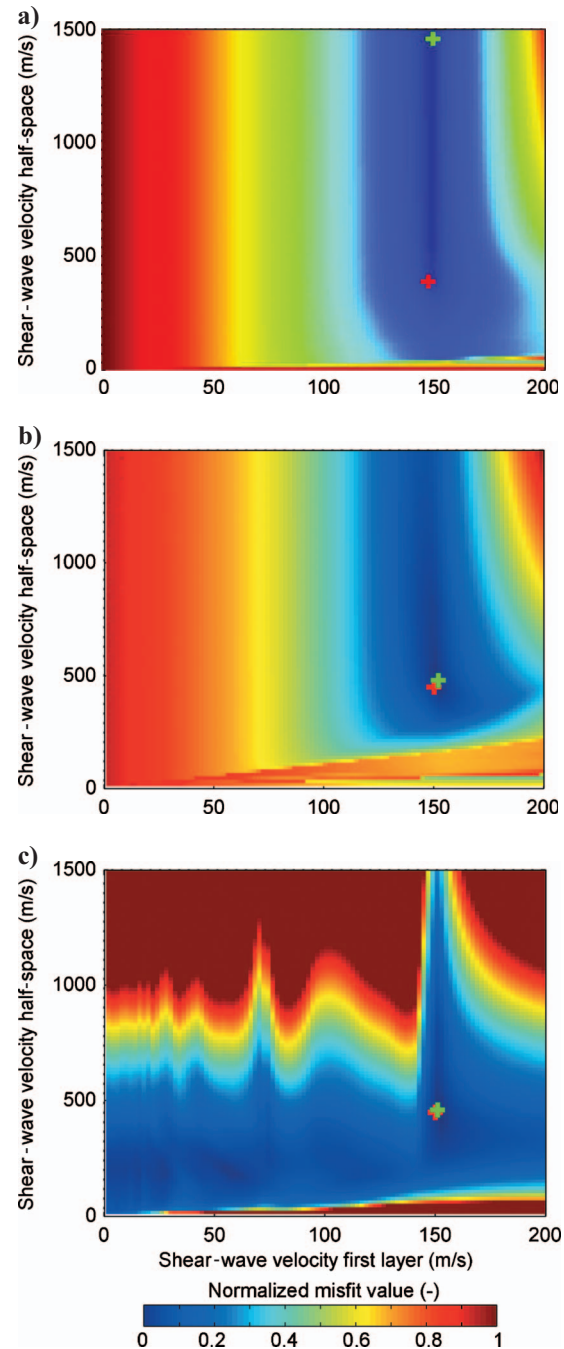

Figure 6. Sensitivity analysis for synthetic case 1. The red crosses represent the theoretical solution; the green crosses represent the function minima. Sensitivity of the classical approach inverting (a) only the slowest branch and (b) all of the branches of the dispersion-curve. (c) Sensitivity of the determinant approach.

branch on, the numbering is incorrect. The presence of the first four correctly identified modes constrains the algorithm to converge to a velocity profile close to the true one.

The result of the inversion with the determinant approach is slightly different. Higher modes of the apparent dispersion curve agree with the correct modal curves of the inverted profile, and the mode jump of the fourth branch is detected. The final model obtained through the determinant inversion is almost coincident with the true model.
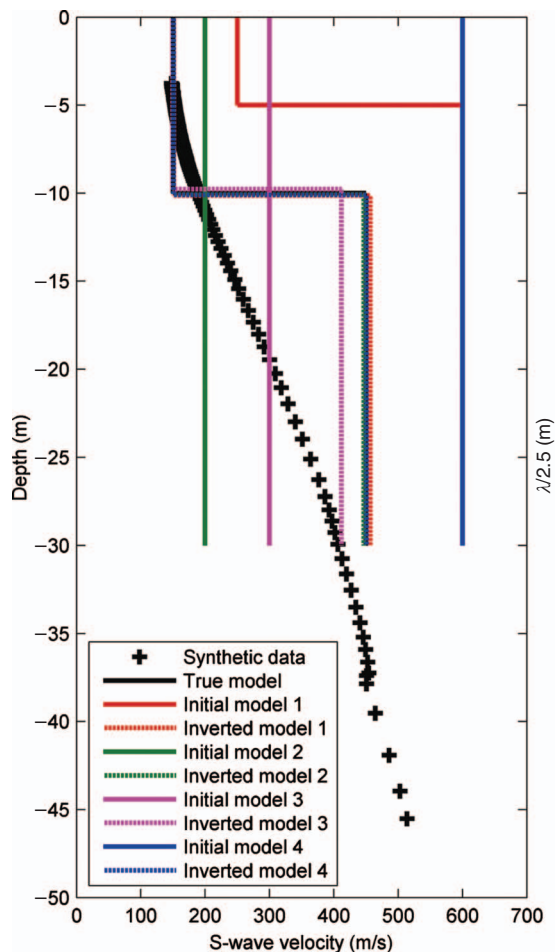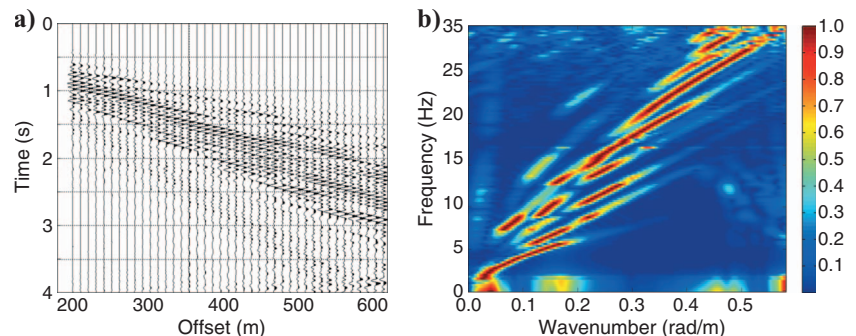

Figure 7. Initial and final models for four inversions of synthetic case 1 using the determinant misfit (colored lines). The S-wave velocity model overestimates the synthetic dispersion-curve ($\lambda/2.5$-V domain) (black crosses).

Figure 8. Representation of (a) the synthetic seismogram and (b) the corresponding f-k spectrum for synthetic case 2.

This example shows that the mode numbering is an important problem even if several branches of the apparent dispersion curve are available because mode jumps may occur also in higher modes.

Two-mode real marine data (site A)

The seismogram used in this example refers to marine data collected for a seismic reflection survey. The water depth is about 30 m, and the source and receivers are 7 m below the water surface. The acquisition parameters are noted in Table 3. We show the seismogram and the f-k spectrum in Figure 10.

The f-k spectrum allows two dispersive events to be identified (Figure 10b). We show the retrieved apparent dispersion curve in Figure 11b. It presents two separate branches in two different frequency bands.

We inverted the experimental dispersion curve using the classical and the determinant approaches (Figure 11). Both inversions fit the two branches of the apparent dispersion-curve well; in each case, the slower branch is associated with the fundamental mode and the other branch is associated with the first higher mode. The two inversions supplied two velocity profiles close to each other, with small differences in the shallow part resulting from the nonuniqueness of the solution.

In this case, no benchmark from other seismic measurements was available; therefore, the quality of the final model was evaluated on the basis of the pattern of the experimental dispersion curve. In general, we can say that the velocity inversion in the shallow part of the model was expected because of the increase of the velocity and the jump to the second mode in the high-frequency band of the apparent dispersion curve. Moreover, the flat branch of the dispersion curve between 10 and 15 Hz presents a velocity of about 800 m/s, in agreement with the shallow, stiff layer retrieved by the determinant inversion and slightly overestimated by the classical inversion. Below this stiff shallow layer, a soft layer is present to a depth of about 120 m; the lower value of the S-wave velocity is about 500–600 m/s. A thick layer with a velocity of about 850 m/s is retrieved from 120 to 680 m depth, where bedrock is encountered.

Two-mode real land data (site B)

These data were collected at Castelnuovo Garfagnana in central Italy (Calosi et al., 2001). The acquisition parameters are noted in Table 3. The subsoil is a stack of layers of different thicknesses composed of sands, silts, and well-graded gravels. Below these layers, a stiff half-space composed of aged clay sands is present. For the site, the results of a downhole test and an S-wave refraction survey were available.

We show an example of the experimental data and the *f-k* spectrum in Figure 12. Based on other geophysical tests, we chose a parameterization made of three layers over a half-space for the inversion. For the first two layers, we imposed a density of 1800 kg/m³; for the stiffer layers below, we imposed a density of 2100 kg/m³. The water table is supposed to be at the first interface.

The apparent dispersion curve is composed of one smooth branch spanning a frequency band from 20 to 100 Hz, with no evidence of jumping on higher modes. We show the results of the classical and the determinant inversions in Figure 13a and b, in terms of soil profile and dispersion curves, respectively. In Figure 13c, we compare the apparent dispersion curve with the misfit surface of the determinant approach; the apparent dispersion curve passes from the fundamental mode to the first higher mode in a region where the two modes are close and the misfit is low.

In the shallower layers, the two inversions produce results that are almost coincident because they are influenced by high-frequency data points belonging to the fundamental mode. Some differences arise in the deeper layers; indeed, the classical inversion retrieves a very stiff half-space in order to fit the apparent dispersion curve with the fundamental mode of the synthetic dispersion curve. The determinant inversion retrieves a lower velocity value for the half-space because it fits the low-frequency part of the apparent dispersion

curve with the first higher mode. This feature has not been predetermined but arises naturally in the determinant inversion. Comparing these results with downhole and refraction results, we can observe that the determinant inversion retrieves a bedrock S-wave velocity that is close to the S-wave velocity of the benchmarks.

Multimode land real data (site C)

We collected these data at Sestri Levante in Liguria, northern Italy. The site is the location of a station of the Italian Accelerometer Network (ITACA), and the survey was performed to implement the Italian strong-motion database (ITACA, 2009). The uppermost layer is a track for the passage of trucks, composed of gravels and pebbles, and a shallow bedrock is expected from geologic information. The acquisition parameters are included in Table 3, and the seismogram and *f-k* spectrum are shown in Figure 14.

The retrieved dispersion curve is composed of one smooth branch, and it presents a velocity increase at high frequency — a common feature when a stiffer layer overlays a soft layer. The initial model is chosen from the plot of the apparent dispersion curve in the $\lambda/2.5$-V domain. We show the results of the inversions using the classical and the determinant misfits in Figure 15.
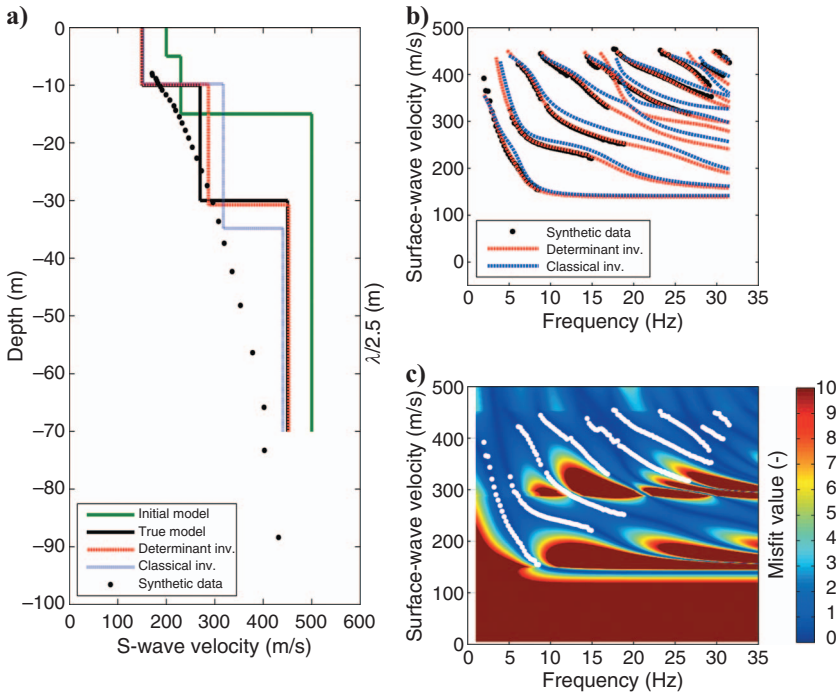

a)
b)
c)

Figure 9. Inversion results for synthetic case 2. (a) S-wave velocity profiles compared with the first branch of the synthetic data ($\lambda/2.5$-V domain). (b) Apparent dispersion curves compared with the calculated dispersion curves for the final models. (c) Apparent dispersion curve compared with the misfit function of the determinant approach.
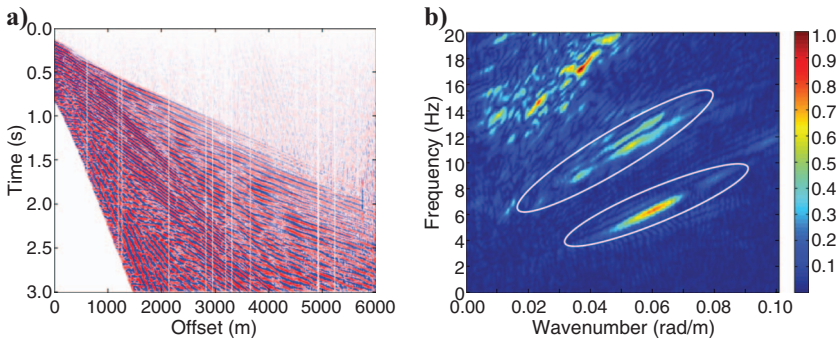

a)
b)

Figure 10. Representation of (a) the recorded seismogram and (b) the corresponding *f-k* spectrum of the seismogram for site A (marine data). The white circles represent the regions where the dispersion curve is picked.

In the classical inversion, the experimental dispersion curve is associated with the fundamental mode because there is no evidence of mode jumps. The retrieved velocity profile presents a small inversion and a very high value of the bedrock S-wave velocity. The data fit is good in the low-frequency band but becomes worse at high frequency. The determinant inversion retrieves a stronger velocity inversion, and the S-wave velocity retrieved for the half-space is more realistic than the one obtained by the classical inversion. The S-wave velocity of the first layer is in agreement with the velocity value of the apparent dispersion curve in the high-frequency band, and the second-layer velocity is in agreement with the lower velocity of the apparent dispersion curve. Data fitting is good (Figure 15c). The apparent dispersion curve fits the modal curves in the part where they are flat, and the jumps from one mode to the following regions where the misfit value is very low.

DISCUSSION

Our new misfit function for surface-wave inversion is characterized by a pattern that allows higher modes to be considered without the need for numbering them. This is especially useful when a smooth passage from one mode to another is present and the experimental dispersion curve is therefore an apparent dispersion curve originated by modal superposition. This kind of situation (mode jumps) occurs quite often when strong velocity contrasts or velocity decreases are present in the velocity profile of the site.

Mode jumps show up at low frequency (passage from fundamental to the first higher mode originated by bedrock contrast) and at high frequency (passage from one higher mode to another higher mode and raising the apparent curve at high frequency originated by stiff top layer). The smooth passage from one mode to another occurs in regions of the frequency/phase-velocity domain, where the modes are close to each other and, even adopting very long receiver arrays, cannot be avoided. Because the passage between the two different modes is usually smooth and the experimental dispersion-curve exhibits a continuous pattern, this effect is seldom recognized in the experimental dispersion-curve. Classical multimodal inversion requires identifying mode jumps before inversion in order to provide the correct results.

The proposed misfit surface has zero values (Figure 1) at modal curves and very low values (not zero) in regions where the mode jumps occur, as observed in Figure 5e around 6 Hz, in Figure 13c around 22 Hz, and in Figure 15c from 50 to 150 Hz. Hence, models that produce modal jumps can represent the minimum of the misfit

Figure 11. Inversion results for site A (marine data). (a) S-wave velocity profiles compared with the first branch of the real data ($\lambda/2.5$-V domain). (b) Dispersion curves. (c) Real dispersion curve compared with the misfit surface of the determinant approach.
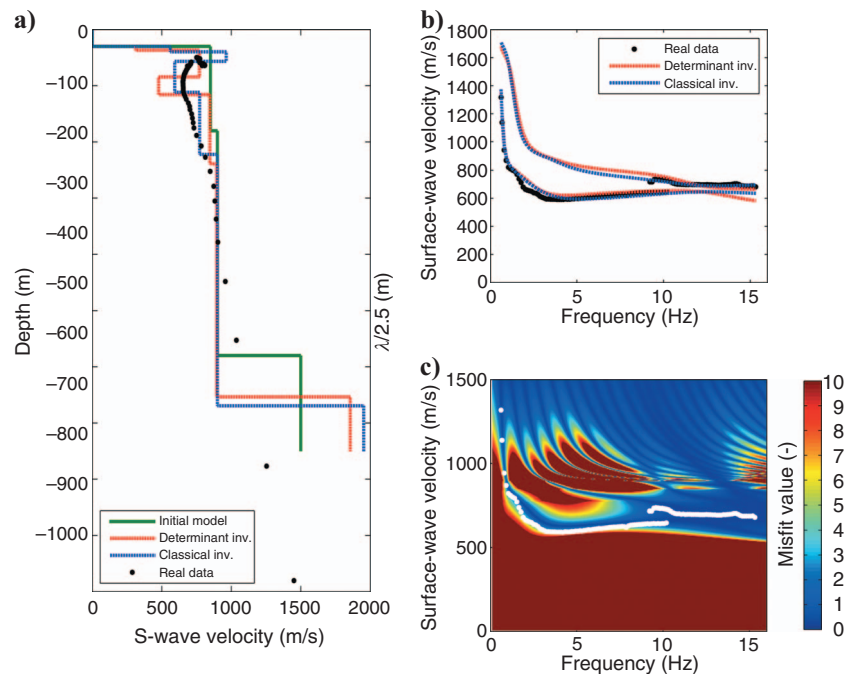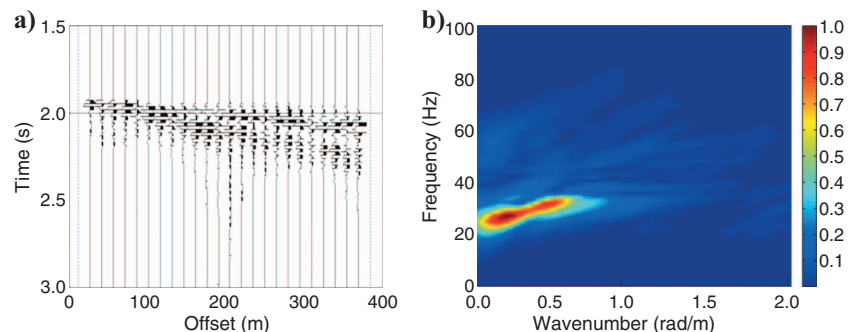

Figure 12. Representation of (a) the recorded seismogram and (b) the corresponding f-k spectrum of the seismogram for site B, Castelnuovo Garfagnana, Italy.

function, as we have shown with the sensitivity analysis performed for synthetic case 1 (Figure 6c). For this reason, the determinant approach handles apparent dispersion curves without the need to simulate the apparent dispersion curve itself.

When only the fundamental mode is retrieved or when mode jumps do not show up and modes are numbered correctly, the determinant inversion supplies the same (or very similar) results as the classical multimodal inversion. The main advantage of the method is reduced computing costs, which are lower for the determinant inversion because dispersion-curve calculation is not required. This aspect would be relevant with respect to more complicated inversion approaches based on the apparent dispersion-curve calculation. The determinant inversion could be considered an alternative to these approaches.

The main drawback of the determinant approach applied to a deterministic inversion is represented by the sensitivity to the initial model. The shape of the misfit surface presents local minima in correspondence with each mode (Figure 6c), and this imposes a careful strategy for initial model selection, e.g., based on the experimental data. For this purpose, we suggest a practical rule consisting of selecting an initial model whose first-layer velocity is higher than the phase velocity of the dispersion curve at high frequency. This rule

has been applied to the presented synthetic and field cases. As with any practical rule, its application cannot be automatic; a careful data evaluation and interpretation, also based on previous knowledge about the site, is required, particularly when the pattern of the dispersion curve is not monotone.

An important feature of the determinant misfit is its nonlinearity with respect to model parameters. The pattern of the misfit surface is steeper in certain regions of the *V-f* domain, where data points are trapped in narrow low-misfit zones and is flatter in other regions; the pattern depends on modal parameters. The pattern of the determinant surface influences the sensitivity of the method with respect to model parameters. Where the surface is steep, the misfit value changes abruptly for small variations of the model; consequently, the method is very sensitive to soil parameters that influence these regions of the determinant surface. On the contrary, in the regions where the surface is flat, the soil model can change with small misfit variations. For normally dispersive profiles (Figures 5e, 9c, and 13c), the determinant values in the low-frequency band is flatter than in the high-frequency band, so the sensitivity of the method with respect to the shallow layers, which influence the high-frequency values of the dispersion curve, is greater than the sensitivity with respect to the deeper layers.
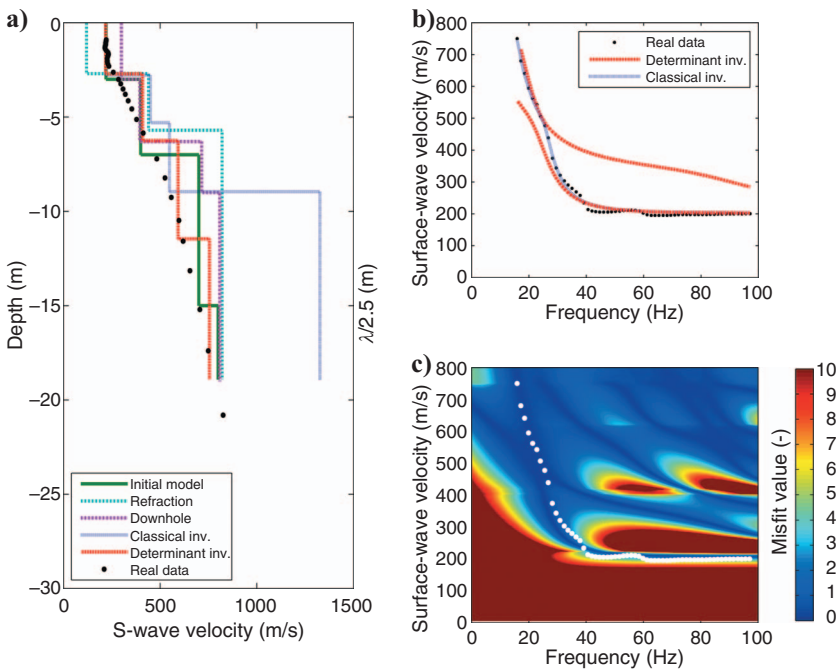

Figure 13. Inversion results for site B, Castelnuovo, Garfagnana, Italy. (a) S-wave velocity profiles compared with the first branch of the real data ($\lambda/2.5$-V domain), a downhole test result, and a refraction result. (b) Dispersion curves. (c) Real dispersion curve compared with the misfit surface of the determinant approach.
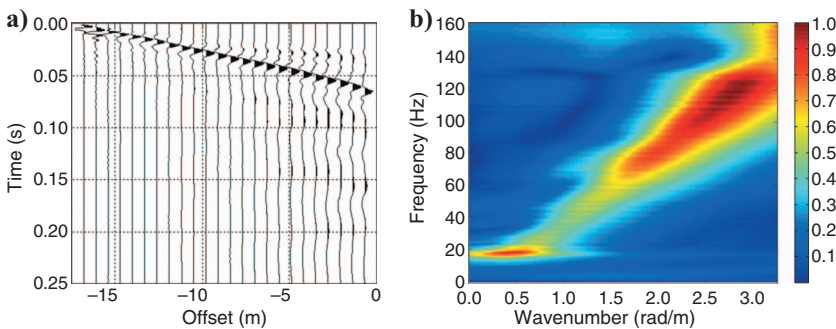

Figure 14. Representation of (a) the recorded seismogram and (b) the corresponding *f-k* spectrum of the seismogram for site C, Sestri Levante, Italy.

Figure 15. Inversion results for site C, Sestri Levante, Italy. (a) S-wave velocity profiles compared with the first branch of the real data ($\lambda/2.5$-V domain). (b) Dispersion curves. (c) Real dispersion curve compared with the misfit surface of the determinant approach.
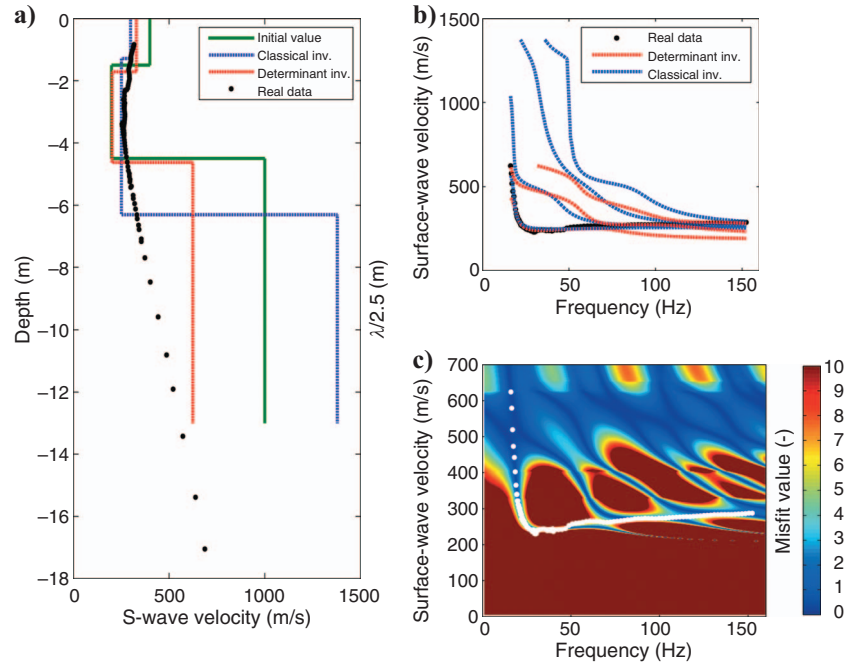
The misfit of a given model increases more if the theoretical dispersion curve does not fit the experimental dispersion curve in the high-frequency band very well than if the theoretical dispersion curve does not fit the experimental dispersion curve in the low-frequency band very well. Consequently, it increases more if the shallow-layer velocity estimate is incorrect than if the deeper-layer estimate is incorrect. This feature has a strong physical significance because surface-wave energy travels near the ground surface. This is related to the fact that surface-wave inversion is a mix-determined problem — overdetermined close to the surface and underdetermined for deeper parts of the model.

In all of the examples considered (Figures 5e, 9c, 11c, 13c, and 15c), the misfit surface of the final model is flat in the regions where mode jumps occur. This feature is useful for the inversion algorithm, helping convergence to the correct solution. In Figures 5e, 13c, and 15c, we can observe a flat region of the misfit surface in correspondence with the passage of the dispersion curve from the fundamental mode to the first higher mode; in Figure 9c, the surface is flat in correspondence with the passage between the fourth- and fifth-higher modes. In Figures 11c and 15c, we can observe that, for subsoil profiles which present velocity inversion, the determinant surface of the best-fitting model is also flat in the high-frequency band, corresponding with the passage to higher modes. In Figure 15c, this behavior is very clear, and we can observe the experimental dispersion curve trapped between the high misfit zones.

CONCLUSIONS

We have proposed an approach for inverting surface-wave data in which the misfit function is a norm of the determinant of the Haskell-Thomson matrix evaluated on the experimental dispersion data points. The main advantage is given by the possibility of taking into account several modes simultaneously, with no need to specify which mode each data point belongs to or to simulate the full waveform. This feature is important for exploration-size surveys because

in this case it may be difficult to perform interpretation such as mode numbering.

On synthetic and field examples, our inversion approach presents advantages with respect to the classical inversion, which considers the distance between velocity vectors of experimental and synthetic dispersion curves.

When it is possible to number the branches of the apparent dispersion curve correctly, classical and determinant inversions lead to similar results, but the computing cost for the determinant inversion is lower. When the identification of mode number is ambiguous on the basis of available information, our method provides an advantage with respect to classical inversion reducing errors in estimating the S-wave velocity profile. When the retrieved dispersion curve should be considered an apparent dispersion curve generated by modal superposition, our proposed approach can handle the inversion, providing the correct final model without the need to perform a full-waveform simulation, which is computationally expensive and requires that one accounts for the proper source wavelet, P- and S-wave attenuation, and receiver response.

The main criticism of the proposed method is related to the presence of several local minima in the misfit function. This feature makes the choice of a consistent initial model very important.

Our inversion process is based on a deterministic approach, but the reduction in computational effort makes the proposed misfit function effective for implementing stochastic algorithms, where many tentative profiles are used.

ACKNOWLEDGMENTS

discussions, and Paolo Bergamo and Claudio Piatti for their help in synthetic model generation. We also thank the associate editor and three anonymous reviewers for their useful and constructive suggestions.

REFERENCES

Buchen, P. W., and R. Ben-Hador, 1996, Free-mode surface-wave computations: Geophysical Journal International, **124**, 869–887.

Calosi, E., M. Ferrini, A. Cancelli, S. Foti, D. Lo Presti, O. Pallara, G. D'Amato Avanzi, A. Pochini, A. Puccinelli, R. Luzi, M. Rainone, and P. Signanini, 2001, Geological and geotechnical investigations for the seismic response analysis at Castelnuovo Garfagnana in central Italy: 15th International Conference on Soil Mechanics & Geotechnical Engineering, Technical Committee 4 Special Volume, 141–148.

Dunkin, J., 1965, Computation of modal solutions in layered, elastic media at high frequencies: Bulletin of the Seismological Society of America, **55**, 335–358.

Dziewonski, A. M., and A. L. Hales, 1972, Numerical analysis of dispersive seismic waves, *in* B. A. Bolt, ed., Methods in computational physics vol. 11: Academic Press, 39–86.

Ernst, F., 2007, Long-wavelength statics estimation from guided waves: 69th Conference and Technical Exhibition, EAGE, Extended Abstracts, E033.

——, 2008, Multi-mode inversion for P-wave velocity and thick near-surface layers: Near Surface Conference, EAGE, Extended Abstracts, A13.

Forbriger, T., 2003a, Inversion of shallow-seismic wavefields: I. Wavefield transformation: Geophysical Journal International, **153**, 719–734.

——, 2003b, Inversion of shallow-seismic wavefields: II. Inferring subsurface properties from wavefield transformation: Geophysical Journal International, **153**, 735–752.

Foti, S., 2000, Multistation methods for geotechnical characterization using surface waves: Ph.D. dissertation, Politecnico di Torino.

Foti, S., L. Sambuelli, L. V. Socco, and C. Strobbia, 2002, Spatial sampling issues in *fk* analysis of surface waves: Proceedings of the Symposium on the Application of Geophysics to Engineering and Environmental Problems (SAGEEP), 12SEI6.

Gabriels, P., R. Snieder, and G. Nolet., 1987, In situ measurements of shear-wave velocity in sediments with higher-mode Rayleigh waves: Geophysical Prospecting, **35**, 187–196.

Ganji, V., N. Gucunski, and S. Nazarian, 1998, Automated inversion procedure for spectral analysis of surface waves: Journal of Geotechnical and Geoenvironmental Engineering, **124**, 757–770.

Gilbert, F., and G. E. Backus, 1966, Propagator matrices in elastic wave and vibration problems: Geophysics, **31**, 326–332.

Gucunski, N., and R. D. Woods, 1992, Numerical simulation of the SASW test: Soil Dynamics and Earthquake Engineering, **11**, no. 4, 213–227.

Haskell, N., 1953, The dispersion of surface waves on multilayered media: Bulletin of the Seismological Society of America, **43**, 17–34.

——, 1964, Radiation pattern of surface waves from point sources in a multilayered medium: Bulletin of the Seismological Society of America, **54**, 377–393.

Herrmann, R. B., 2002, SURF code, http://www.eas.slu.edu/People/RBHerrmann/, accessed 29 April 2010.

Herrmann, R. B., and C. Y. Wang, 1980, A numerical study of p-, sv- and sh-wave generation in a plane layered medium: Bulletin of the Seismological Society of America, **70**, 1015–1036.

ITACA Working Group, 2009, Data base of the Italian strong motion records, Italian Accelerometric Archive, http://itaca.mi.ingv.it, accessed 1 May 2010.

Kausel, E., and J. M. Roesset, 1981, Stiffness matrices for layered soils: Bulletin of the Seismological Society of America, **71**, 1743–1761.

Kennett, B., and N. Kerry, 1979, Seismic wave in a stratified half space: Geophysical Journal of the Royal Astronomical Society, **84**, 557–583.

Kennett, B., 1974, Reflection, rays and reverberation: Bulletin of the Seismological Society of America, **64**, 1685–1696.

Lai, C. G., and G. J. Rix, 1999, Inversion of multi-mode effective dispersion-curves, *in* M. Jamiolkowski, R. Lancellotta, and D. Lo Presti, eds., Prefailure deformation characteristics of geomaterials: Balkema, 411–418.

Lu, L., and B. Zhang, 2006, Inversion of Rayleigh waves using a genetic algorithm in the presence of a low-velocity layer: Acoustical Physics, **52**, 701–712.

Luo, Y., Y. Xu, Q. Liu, and J. Xia, 2008, Rayleigh-wave dispersive energy imaging and mode separating by high resolution linear Radon transform: The Leading Edge, **27**, 1536–1542.

Maraschini, M., 2008, A new approach for the inversion of Rayleigh and Scholte waves in site characterization: Ph.D. dissertation, Politecnico di Torino.

Maraschini, M., F. Ernst, D. Boiero, S. Foti, and L. V. Socco, 2008, A new approach for multimodal inversion of Rayleigh and Scholte waves: 70th Conference and Technical Exhibition, EAGE, Extended Abstracts, D036.

Mari, J. L., 1984, Estimation of static corrections for shear-wave profiling using the dispersion properties of Love waves: Geophysics, **49**, 1169–1179.

McMechan, G. A., and M. J. Yedlin, 1981, Analysis of dispersive waves by wave field transformation: Geophysics, **46**, 869–874.

Nolet, G., and G. F. Panza, 1976, Array analysis of seismic surface waves: Limits and possibilities: Pure and Applied Geophysics, **114**, 5775–5790.

Park, C., R. D. Miller, and J. Xia, 1998, Imaging dispersion-curves of surface waves on multichannel records: 68th Annual International Meeting, SEG, Expanded Abstracts, 1377–1380.

——, 1999, Multimodal analysis of high frequency surface wave: Proceedings of the Symposium on the Application of Geophysics to Engineering and Environmental Problems (SAGEEP), 115–122.

Ryden, N., and C. B. Park, 2006, Fast simulated annealing inversion of surface waves on pavement using phase-velocity spectra: Geophysics, **71**, no. 4, R49–R58.

Socco, L. V., and C. Strobbia, 2004, Surface wave methods for near-surface characterisation: A tutorial: Near Surface Geophysics, **2**, no. 4, 165–185.

Song, X., and H. Gu, 2007, Utilization of multimode surface wave dispersion for characterizing roadbed structure: Journal of Applied Geophysics, **63**, no. 2, 59–67.

Tarantola, A., 2005, Inverse problem theory and methods for model parameter estimation: Society for Industrial and Applied Mathematics.

Thomson, W. T., 1950, Transmission of elastic waves through a stratified solid medium: Journal of Applied Physics, **21**, 89–93.

Tokimatsu, K., 1997, Geotechnical site characterization using surface waves: Proceedings of the 1st International Conference on Earthquake Geotechnical Engineering, 1333–1368.

Tokimatsu, K., S. Tamura, and H. Kojima, 1992, Effects of multiple modes on Rayleigh wave dispersion characteristics: Journal of Geotechnical Engineering, **118**, 1529–1543.

Xia, J., R. D. Miller, C. B. Park, and G. Tian, 2003, Inversion of high frequency surface waves with fundamental and higher modes: Journal of Applied Geophysics, **52**, no. 1, 45–57.

Xu, Y., J. Xia, and R. D. Miller, 2006, Quantitative estimation of minimum offset for multichannel surface-wave survey with actively exciting source: Journal of Applied Geophysics, **59**, no. 2, 117–125.

Zhang, S. X., and L. S. Chang, 2003, Possible effects of misidentified mode number on Rayleigh wave inversion: Journal of Applied Geophysics, **53**, no. 1, 17–29.